Enhanced Ab Initio Molecular Dynamics Exploration Unveils the Complex Role of Different Intramolecular Bases on the Water Nucleophilic Attack Mechanism

Schilling, Mauro ; Cunha, Richard A ; Luber, Sandra

Abstract: Rational design of water oxidation catalysts (WOCs) is a valuable complement to the traditional empirically driven approach used to improve the catalytic performance of existing catalysts. The validity of those predictions depends on the applied simulation protocol and its capability to account for all relevant aspects of the catalytic system. Commonly used approaches often only include an approximative treatment of solute-solvent interactions and neglect dynamic effects occurring at ambient temperature. In order to go beyond those limitations, we rely on a density functional theory-based molecular dynamics (DFT-MD) simulation protocol, which shows that the inclusion of those effects is essential in order to understand the O–O bond formation process in various facets. In this work, we focus on the effects of a modification to the Py5 ligand framework of a Ru-based WOC. Previously, it was suggested that increasing the basicity of the pyridyl subunit results in a lower activation barrier for the O–O bond formation [Dalton Trans.2018, 47, 10780–10490]. We take advantage of the metadynamics method to efficiently explore the O–O bond formation event using DFT-MD. This allows us not only to investigate in detail the beneficial effect an increased basicity has on the O–O bond formation but also to rationalize its origin and complexity that is in part found in the structure of the first solvation shell of the catalyst.

DOI: https://doi.org/10.1021/acscatal.0c01422

Enhanced Ab Initio Molecular Dynamics Exploration Unveils the Complex Role of Different Intramolecular Bases on the Water Nucleophilic Attack Mechanism

Mauro Schilling , Richard A. Cunha , and Sandra Luber* *

University of Zurich, Department of Chemistry, Winterthurerstrasse 190, CH-8057 Zürich, Switzerland

E-mail: sandra.luber@chem.uzh.ch

Table of Content

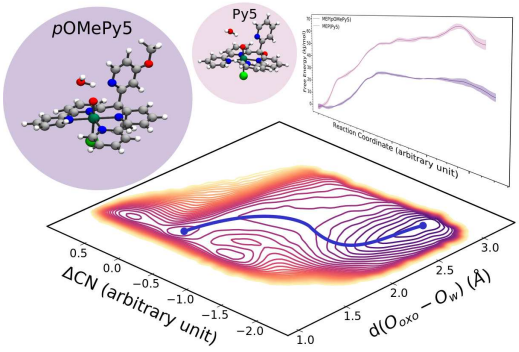

Abstract

Rational design of water oxidation catalysts (WOCs) is a valuable complement to the traditional empirically driven approach used to improve the catalytic performance of existing catalysts. The validity of those predictions depends on the applied simulation protocol and its capability to account for all relevant aspects of the catalytic system. Commonly used approaches often only include an approximative treatment of solute-solvent interactions and neglect dynamic effects occurring at ambient temperature. In order to go beyond those limitations we rely on a density functional theory based molecular dynamics (DFT-MD) simulation protocol which shows that the inclusion of those effects is essential in order to understand the O−O bond formation process in various facets. In this work we focus on the effects of a modification to the Py5 ligand framework of a Ru-based WOC. Previously, it has been suggested that increasing the basicity of the pyridyl subunit results in a lower activation barrier for the O−O bond formation [Dalton Trans. 2018, 47, 10780-10490]. We take advantage of the metadynamics method to efficiently explore the O−O bond formation event using DFT-MD. This allows us not only to investigate in detail the beneficial effect an increased basicity has on the O−O bond formation, but also to rationalize its origin and complexity that is in part found in the structure of the first solvation shell of the catalyst.

Keywords: water oxidation, homogeneous catalysis, density functional theory, artificial photosynthesis, molecular dynamics, enhanced sampling

Introduction

The development of renewable energy sources is one of the greatest challenges faced by our society. Among the many possible solutions, artificial water splitting promises to be particularly viable since its products can be used as 'green' fuel. The chemical reactions associated with this process are the water oxidation and the water reduction, for which specific catalysts have been developed. In-depth knowledge of the electronic structure of

those catalysts and the underlying reaction mechanisms are a prerequisite for informed design of novel catalysts.

In a previous study we had investigated in detail the kinetics and thermodynamics of a Ru-based water oxidation catalyst (WOC) bearing a pentapyridyl ligand (Py5R = 6,6″–(R-(pyridin–2–yl)methylene)di–2,2′-bipyridine), where R is either a methyl or methoxyl substituent (see Figure 1).[1,2] The combination of both experimental results and simulations applying density functional theory (DFT) allowed us to rationalize how a seemingly chemically innocent ligand modification can alter the catalytic performance. We confirmed that the O–O bond formation, that is commonly assumed to be the rate-limiting step of the water oxidation process, was hardly effected by the nature of the ligand. On the other hand, the dissociation of the chlorido ligand turned out to be different amongst the two (see Figure 1).[1,2] Intrigued by this observation, we computationally screened a series of chemical modifications of the dangling pyridyl subunit. Such moiety is expected to act as an intramolecular base which enhances the nucleophilicity of the water molecule, that in a water nucleophilic attack (WNA) mechanism forms the O–O bond with the metal-oxo species.[2] The introduction of an intramolecular base is a design criteria that is known to facilitate the O–O bond formation.[3–6] We found a correlation of the activation energy on the sterical demand and the electron donating or withdrawing effect of the substitutes. The most promising modification turned out to be a methoxyl group in *para* position to the nitrogen atom of the pyridyl subunit **{Ru(*p*OMePy5OMe)}** (see Figure 1).[2] Please note, to this date **{Ru(*p*OMePy5OMe)}** has not yet been sythesized.

Modifying the ligand framework of existing catalysts in order to improve their efficiency has also been used in other *in silico* design studies.[7] The highly efficient WOCs developed by Sun and co-workers featuring e.g. the bda (2,2′-bipyridine-6,6′-dicarboxylic acid) ligand were studied in great depth and various modifications to the ligand-framework were proposed.[8–12] Other polypyridine based mononuclear Ru-based WOCs were studied as well.[13–16] The identification of the appropriate descriptors to compare properties of the different catalysts is

often challenging and requires in depth knowledge of the WOCs and its properties, as it is the case for the catalysts at hand.[2,17,18]

The methods commonly used in the field are based on DFT geometry optimizations. This was also applied in our previous study[2] where the conductor-like-screening-model (COSMO)[19,20] was used to approximately account for solvent-solute interactions. Such an approach does not allow to fully account for ambient temperature and environmental effects.[21–26] This approach will be referred to as static-DFT in the following.

Recently, we therefore went beyond common restrictions of static-DFT approaches by using DFT-based molecular dynamics (MD) simulations, also known as *ab initio* molecular dynamics (AIMD), to model the O−O bond formation for **{Ru(Py5OMe)}**, the native form of the WOC, in a box of explicit water molecules.[27] To facilitate the observation of this rare event, we took advantage of enhanced sampling techniques such as *Bluemoon*[28–30] and well-tempered metadynamics (WT-MetaD).[31–35] Those simulations allowed us to dissect the complexity of the O−O bond formation by a WNA where multiple bonds are broken and formed at the same time. Furthermore, we showed that the intramolecular base plays a crucial role in the chemical reaction at hand, and that a base-assisted WNA is the energetically favorable pathway.[27] The availability of a proton acceptor such as a pyridine or carboxylate allowed in several cases the determination of the activation barrier without the use of sampling methods.[2,5,36–38] However, those static-DFT approaches often require the inclusion of several solvent molecules that act as proton relays and results can be biased by the initial guess for the geometry optimization.

The complexity and size of most WOCs limit the application of computationally demanding enhanced sampling techniques using AIMD. Nonetheless, there are several examples where the O−O bond formation has been studied. A base-independent WNA on the oxo-ligand of a Ru-based WOC was studied by Vallés-Pardo *et al.*[39] and Piccinin *et al.*[40] In both works MetaD is used to facilitate the O−O bond formation. For the two systems, a mono-nuclear transition metal complex and a tetranuclear polyoxometalate that

follows a single-site mechanism, activation energies of 102 kJ/mol[39] and 94 kJ/mol[40] were reported. This is significantly larger than the activation energy of 69 kJ/mol reported for **{Ru(Py5OMe)}**, highlighting the importance of an appropriate proton acceptor.[27] Govindarajan *et al.* simulated the WNA and its associated hydrogen bonding network by the *Bluemoon* method, where they find the activation energy for the O−O bond formation unaffected by an additional solvent molecule that acts as proton relay.[41] In two consecutive studies, Shao *et al.* used the *Bluemoon* method to model the WNA where either a solvent molecule or a hydroxide act as the proton acceptor. Some analogies to the current work will be discussed later (see Section Characteristics of the FES).[42,43]

Besides the WNA, the interaction of two metal oxo species (I2M), sometimes also referred to as radical coupling (RC), is a common proposed mechanism for the O−O bond formation and was studied employing e.g. the empirical valence bond (EVB) model.[44,45] Due to the spatial requirements of the Py5-ligand the I2M was not considered for **{Ru(Py5OMe)}**.[1,2] Other proposals for mechanisms studied by enhanced sampling methods can be found in Refs.[46,47] It is worth mentioning that studies on Ru-based WOCs, that possess a similar polypyridyl based ligand framework, have suggested that the metal oxo-species can undergo an oxygen-atom transfer reaction with its pyridyl ligands forming a metal coordinated pyridyl-N-oxide.[46,48–50] An analogue reaction could also be imagined in the case of the Py5-based WOCs, but has not been considered so far in previous studies and is beyond the scope of the current study.

In this study we perform forefront well-tempered metadynamics (WT-MetaD)[33] simulations based on AIMD for **{Ru(*p*OMePy5OMe)}**, thus combining the *in silico* design approach with a sophisticated dynamic computational approach for the description of the solvent-solute interactions and other effects beyond the commonly used static picture assuming a temperature of 0 K. In doing so we elucidate in detail the effect of the increased basicity of the dangling pyridine on the O−O bond formation. Having already performed analogous simulations for the native form of the WOC, namely **{Ru(Py5OMe)}**, does allow for a

direct comparison of the two WOCs and quantification of the differences, which provides valuable novel insight as a basis for informed design of such catalysts.

Methods

Computational Settings

All AIMD simulations were performed employing the CP2K program package (revision 18464).[51] All atoms were described by the DZVP-MOLOPT-SR-GTH basis sets[52] as well as the corresponding GTH-PBE pseudo potentials.[53] The Perdew-Burke-Ernzerhof (PBE) exchange-correlation functional[54] together with Grimme's D3 dispersion correction,[55] and a cutoff of 800 Ry for the auxiliary plane wave basis set were used. The simulations were performed in the NVT ensemble with a time-step of 0.5 fs, where the temperature was kept constant at 300 K by a Nosé-Hoover chain thermostat.[56,57] Those are the same settings as the ones used in our previous study.[27] For all simulations a cubic simulation cell with a side length of 14.56 Å, that contains the metal-oxo species of the catalyst ($[Ru^{V}O(pOMePy5OMe)Cl]^{2+}$) as well as 107 H_2O molecules, was employed. Initially, the size of the simulation cell was determined for the unmodified catalyst ($[Ru^{V}O(Py5OMe)Cl]^{2+}$) through NPT simulations at 1 bar and 300 K, subsequent equilibration at 300 K in the NVT ensemble resulted in the initial structures for the enhanced sampling calculations. Relevant structural representations of the different intermediates were obtained by employing the clustering algorithm implemented in the VMD[58] plugin METAGUI.[59]

For a number of selected frames that are representative of the O−O bond formation localized molecular orbitals (LMOs) were obtained using Turbomole version 7.3.[60] For this purpose, all solvent molecules were removed and only the catalysts and the nucleophile were considered. The LMOs were obtained at the BP86-D3/def2-TZVP[61–63] level of theory applying the Forster-Boys localization.[64] Relevant LMOs were identified by the Mulliken contributions ($> 10\%$) of the atoms involved in the bonds of interest i.e. Ru−O_{oxo}, O_{oxo}−O_w,

O_w-H and $N-H$ for the labeling of the atoms, see Figure 1). The same LMO analysis was also performed at the PBE-D3/def2-TZVP level of theory, where we find only minor differences compared to the results obtained with BP86-D3 (see Figure S5 and S6 in the Supplementory Information). In addition the shared electron numbers (SENs) were analyzed for these bonds. This analysis is based on modified atomic orbitals, that were obtained using the default settings in Turbomole.[65]

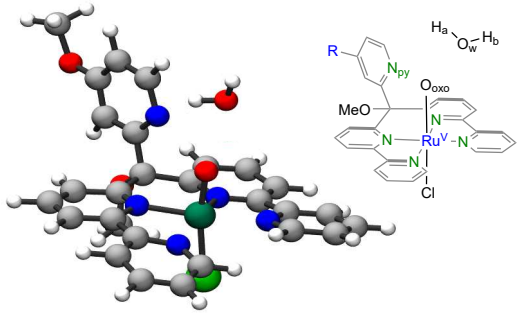

Figure 1: Ball-stick visualization of **{Ru(*p*OMePy5OMe)}** and a single solvent molecule that acts as the nucleophile. For clarity sake no other solvent molecules are shown.

Metadynamics

All MetaD simulations were performed using PLUMED (version 2.4.3),[66] together with CP2K(revision 18461).[51] In order to facilitate the sampling, we used six independent walkers all of which contributed to the same metadynamics bias potential.[67] Further, the WT-MetaD formalism together with rigorous error analysis was used to enforce the convergence of the simulation.[33] Initially, Gaussians with a height of 1 kJ mol^{-1} were added to the bias potential at a pace of 50 steps (i.e. every 25 fs). The bias factor (γ) of the WT-MetaD was set to 25 in order to allow the sampling of barriers with a height of approx. 60 kJ mol^{-1}. In addition, depending on the employed CV, restraining potentials were added in order to limit the sampling space to a meaningful one (see Section 'Restraining Potentials' in the Supplementary Information). For further details on the simulation protocol see Ref.[27] In the course of this work

we performed some additional post-processing on the previously published data[27] in order to allow for direct comparison with the MetaD simulations of **{Ru(*p*OMePy5OMe)}**.

Results and Discussion

In the following sections we will describe the O−O bond formation for **{Ru(*p*OMePy5OMe)}** and the differences in this reaction when the reaction is catalyzed by **{Ru(Py5OMe)}**. To assure the validity of the comparison we employ the same simulation protocol as in our previous study.[27] The collective variables (CVs) used to describe the reaction are the distance of the oxo-ligand (O_{oxo}) and the oxygen of the nucleophile (O_w) d($O_{oxo}-O_w$) (CV1) and the difference in the coordination number (CN) of the base (CN(NH)) and the nucleophile (CN(O_wH)), Δ(CN(NH)−CN(O_wH)) (CV2). While CV1 is used to monitor the bond formation, CV2 keeps track of the proton transfer (see Figure S1 in the Supporting Information for a graphical representation of WOCs and the labeling of the key fragments). Analogous system specific definitions of the CVs had already been successfully applied previously.[40]

In our previous study we had thoroughly assessed the convergence of the MetaD simulation.[27] Here, we apply the same standards defined there. The strongest indication of the convergence of the simulation is the reoccurrence of the O−O bond formation event within multiple individual walkers (see Figure 2). Further, projecting the free energy surface (FES) onto the degrees of freedom that were biased over the course of the MetaD simulation can give an indication of convergence (see Figure 3 and Figure S2). Standard deviations were obtained as described in our previous work, by performing block averages over the concatenated trajectory of the six individual walkers.

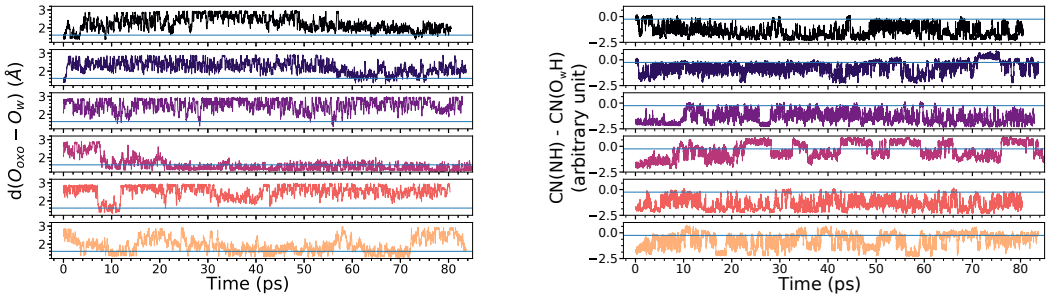

Figure 2: Left: Time-trace of the O_{oxo}–O_w distance for different walkers of **{Ru(*p*OMePy5OMe)}**. The blue horizontal line indicates the formation of the O–O bond. Right: Time-trace of CN(NH) - CN(O_wH) of the same simulation. Formation of the hydroperoxo species is indicated by the horizontal blue line. Note the horizontal lines merely serve as a visual guideline rather than a strict assignment of states.

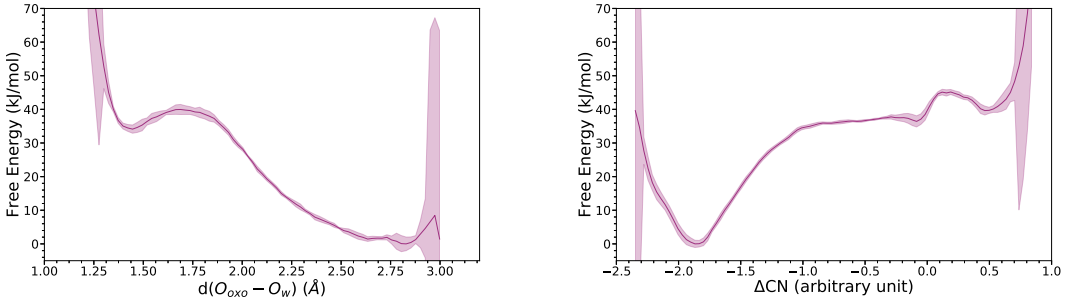

Figure 3: Left: One-dimensional free energy profile as a function of the O_{oxo}–O_w distance for **{Ru(*p*OMePy5OMe)}** and its respective standard deviation. Right: One-dimensional free energy profile as a function of the CN(NH) – CN(O_wH) CV of the same simulation. Note the free energy profiles shown here were obtained by reweighting procedures accounting for the additional bias imposed by the restraining potentials.

Characteristics of the FES

Minimum energy pathways (MEPs) on the reconstructed FES describing the O–O bond formation event were obtained by using minimum energy pathway analysis for energy landscapes (MEPSA).[68] The standard deviation of the MEP was obtained by projecting the final MEP on the FESs of the block analysis method (see Figure 4, 4 blocks used, and Figure S3). The FES reconstructed from the MetaD simulation of **{Ru(*p*OMePy5OMe)}** explores analogues intermediates as the one described for **{Ru(Py5OMe)}** in Ref.[27](see Figure 5).

The MEP describes the formation of the O–O bond by starting from the reactant (R), where the nucleophile and the catalyst do only weakly interact. Hydrogen bonding of the nucleophile to the intramolecular base leads to a pre-orientation of the nucleophile in the so-called associated reactant (AR) state. From there, in a concerted manner the O_{oxo}–O_w and the N–H bond are formed, and the O_w–H bond is broken leading to the transition state (TS) and the desired product (P), a hydro-peroxo species. The P state itself is prone to proton-reshuffling reactions. The latter takes place between the base and the hydro-peroxo ligand as well as the surrounding solvent. This leads to the formation of the deprotonated base-assisted state (P1) where one proton is transfered to the solvent while the other is shared among the base and the ligand. Upon transfer of the shared proton to either the ligand or the base, the base-independent product (P3) or the peroxo species (P2) is formed. The spontaneous deprotonation of the hydro-peroxo species has also been observed by Shao *et al.* independently of the nature of the proton acceptor i.e. H_2O or OH^-.[42,43] The P2 species is the next intermediate towards the release of molecular oxygen. The corresponding CV2 value of 0.5 indicates that there is still significant hydrogen bonding between either the protonated base or solvent molecules, which goes along with an average d(O_{oxo}–O_w) distance of 1.21 ± 0.07 Å, that is closer to molecular hydroperoxide (1.47 Å) than to molecular oxygen (see Tables S3 and S4 in the Supplementary Information for a further characterization of the P2 state).[42,69]

Comparing the energetics of the MEPs reveals a clear preference for **{Ru(*p*OMePy5OMe)}** over **{Ru(Py5OMe)}**, as suggested by our earlier study applying static DFT simulations (see Table 2 and Figure 6).[2] The difference between the two MEPs is caused primarily by the breakage of the O_w–H bond and the formation of the N–H bond, respectively. In the case of **{Ru(*p*OMePy5OMe)}** this happens at larger O_{oxo}–O_w distances suggesting a stronger interaction of the base and the nucleophile. The deprotonation of the nucleophile facilitates the O–O bond formation, as can be seen from the energetic plateau that is reached when the proton is shared between the nucleophile

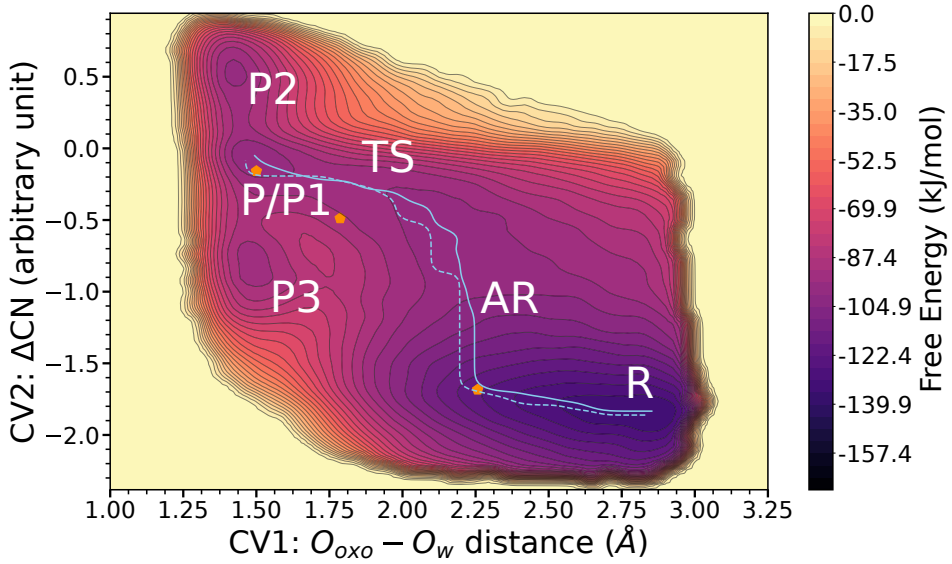

Figure 4: Visualization of the MEP for the O–O bond formation on the FES of **{Ru(*p*OMePy5OMe)}** (solid line) and **{Ru(Py5OMe)}** (dashed line) both following the base-independent mechanism. The orange pentagons correspond to the AR, TS and P state of **{Ru(*p*OMePy5OMe)}** obtained by the static DFT simulations reported by Schilling *et al.*[2]

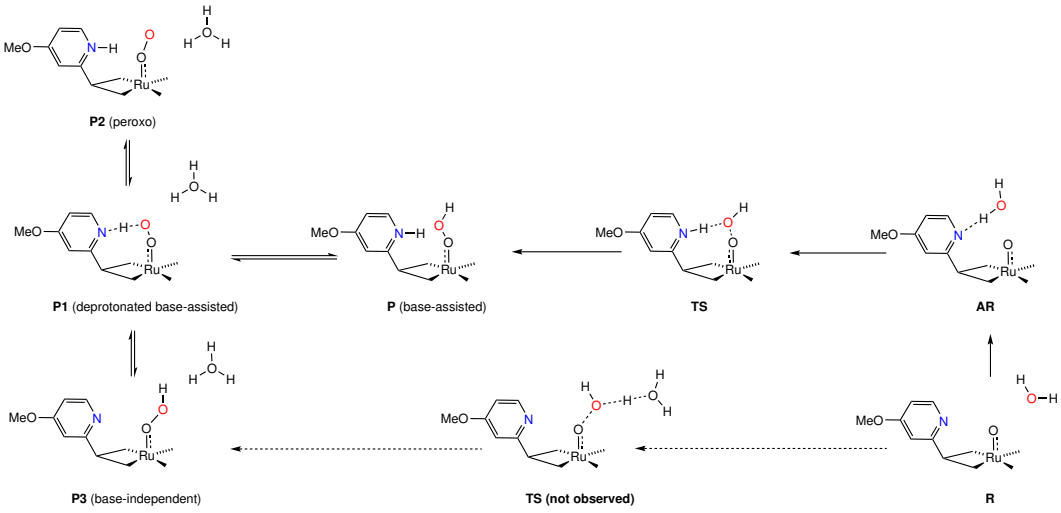

Figure 5: Schematic overview of the reaction network connecting the observed states. Note that P and P1 co-inhabite the same free energy basin in our simulation and thus are virtually indistinguishable.

and the base (CV2 ≈-0.75) (see Figure 4). At this stage the O – O bond formation is almost barrier free due to the proper spatial orientation of the nucleophile. This is not the case for **{Ru(Py5OMe)}** where a clear energetic difference between the pre-oriented nucleophile and the transition state was found.[27]

In the case of **{Ru(Py5OMe)}** inspection of the FES suggested the base-independent WNA to be energetically comparable to the base-assisted WNA.[27] However, for **{Ru(*p*OMePy5OMe)}**, the base-assisted pathway is energetically favorable by more than 10 kJ/mol. The energetic inequality of the two pathways can also be shown by reweighting the FES using a three-dimensional reaction coordinate. By means of reweigthing one can rewrite the FES in any reaction coordinate that is a function of the atomic position. The more uncorrelated the new reaction coordinate is with respect to the ones biased the larger would be the error in the statistical description of said coordinate. Here the protonation state of the base, represented by the CN(NH), is used to understand if the reaction can occur in a base independent pathway since this CV is highly correlated to the biased ones. A base independent pathway is energetically unfavorable, as can be seen from the FESs where the MEP connecting the R and P state involves the protonation of the base, while there is no lower energy passage connecting R and P3 (see Figure 7).

In our previous work, we compared the energetics of the extrema obtained by static DFT calculations with the ones from the MEP analysis of the FES as well as those from the projected FES.[27]

A direct comparison of the activation energies obtained by static-DFT employing implicit solvation and AIMD simulations using explicit solvation is not straight forward. On the one hand, both methods use different levels of approximations to account for solute-solvent interactions. On the other hand, AIMD naturally includes the dynamics of both the solvent and the solute at a given temperature that are not accounted for in static-DFT. In order to allow a comparison between the two methods we do not only compare the energetics, but more importantly we project the structures obtained by static-DFT onto the FES in order to

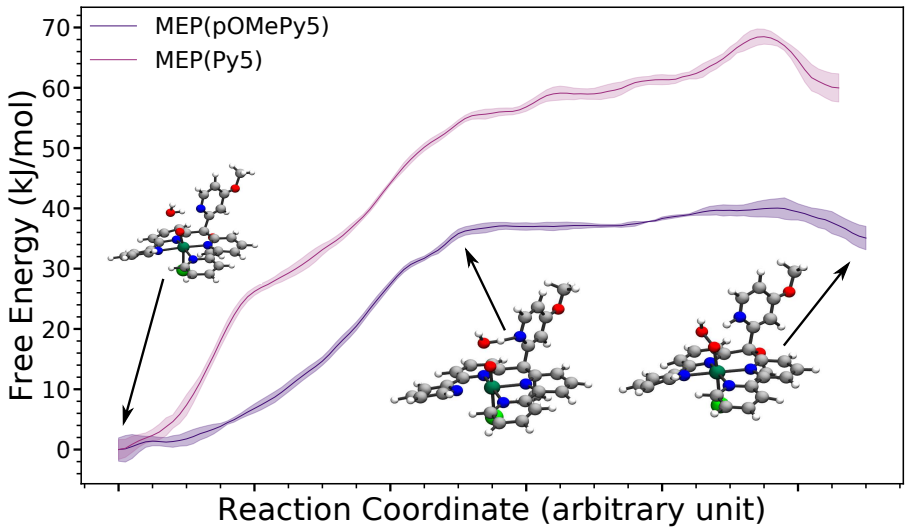

Figure 6: MEP of the base-assisted O−O bond formation of **{Ru(*p*OMePy5OMe)}** and **{Ru(Py5OMe)}** obtained from the MetaD simulations. An estimation of the error of the MEP is shown together with exemplary structures along the reaction coordinate. Those were obtained by the clustering algorithm implemented in METAGUI 3.0.[59] For clarity sake only the nucleophile is shown.

evaluate their energies at the same level of theory (see Schilling *et al.* for a more exhaustive comparison of the methodologies).

Both studied compounds, **{Ru(Py5OMe)}**,[27] and **{Ru(*p*OMePy5OMe)}**, show a reasonable agreement of their energetics and structures among the two vastly different methods. The main difference is the relative stability of the P state, which was identified to be over-stabilized in the static DFT approach (see section 'Structural Features of the Extrema' in the Supplementary Information for a detailed comparison of the structural features). Comparing the activation energies of the O−O bond formation of the two catalysts obtained by the different methodologies reveals that in all cases **{Ru(*p*OMePy5OMe)}** is superior to **{Ru(Py5OMe)}** (see Table 2). This effect is stronger within the MetaD framework as can be seen from the free energy differences of the TS state among the two catalysts ($\Delta TS_{H-OMe} = 29 \pm 3$ kJ/mol, where H represents **{Ru(Py5OMe)}** and OMe stands for **{Ru(*p*OMePy5OMe)}**) than in the case of the static DFT simulations

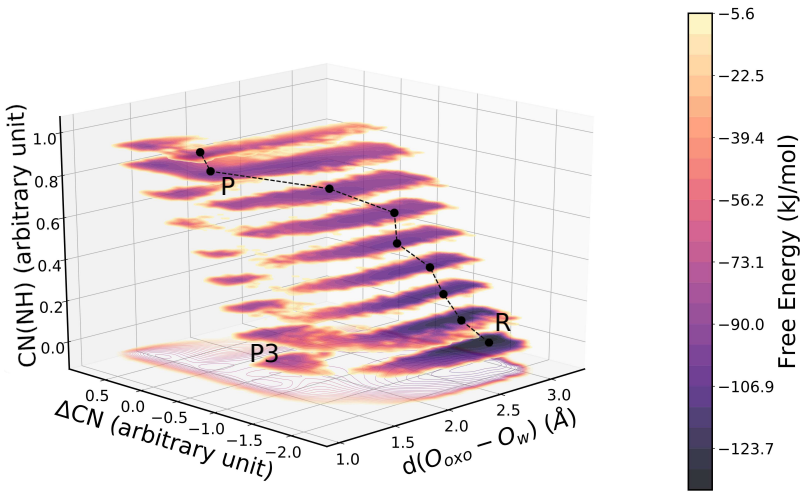

Figure 7: FES of **{Ru(*p*OMePy5OMe)}** reconstructed using the biased CVs (CV1 and CV2) as the x- and y-axes. Additionally, a third dimension, the coordination number of the base nitrogen with any hydrogen (CN(NH)) (z-axes), is used to visualize the preferred reaction path. Note that the path shown in the graph only serves as a visual aid and does only qualitatively correspond to the MEP shown in Figure 4.

(ΔTS_{H-OMe} = 16 kJ/mol). This difference is in part reflected by the relative stability of the AR projected on the FES ($\Delta AR_{H-OMe} = 17 \pm 2$ kJ/mol). This suggests that in case of **{Ru(*p*OMePy5OMe)}** the increased basicity leads to an energetically favorable pre-orientation of the nucleophile prior to the O−O bond formation. Employing *Bluemoon*[28] simulations, it was shown recently that not only intramolecular bases but also the introduction of a basic molecule such as hydroxide in the solvation shell leads to lower activation barriers for a WNA.[43] In these simulations the TS was localized at a larger O−O distance indicating a stronger interaction between the nucleophile and the oxo-species. This is reminiscent of the MetaD simulations discussed here where the O−O distance in the TS is elongated in the case of **{Ru(*p*OMePy5OMe)}**. Shao *et al.* also reported a significant stabilization of the P state with respect to the TS, which is likely attributed to the protonation of the anionic solvation shell.[43] This is not the case for the WOCs studied in this work, where the solvation shell is either neutral or cationic upon protonation.

Table 1: Free energy differences for the R, AR, TS and P state obtained from the MEP of the FES. Standard deviations are given for all free energies obtained from a statistical ensemble. All values given are in kJ/mol.

	R	AR	TS	P
static **{Ru(Py5OMe)}**[2]	0	29	65	26
static **{Ru(*p*OMePy5OMe)}**[2]	0	26	49	13
static on FES **{Ru(Py5OMe)}**[27]	0	31 ± 1	72 ± 2	63 ± 2
static on FES **{Ru(*p*OMePy5OMe)}**	0	14 ± 2	45 ± 2	38 ± 2
MEP **{Ru(Py5OMe)}**[27]	0 ± 2	-	69 ± 2	62 ± 2
MEP **{Ru(*p*OMePy5OMe)}**	0 ± 2	-	40 ± 2	35 ± 2

The Effect of the Increased Basicity

The main difference between **{Ru(*p*OMePy5OMe)}** and **{Ru(Py5OMe)}** is the increased basicity of the pyridyl subunit. This can be rationalized by the fact that the introduction of a methoxy group in the *para* position of a pyridine leads to an increase of its basicity by 1.5 pK_a units.[70] The pK_a value of the dangling pyridyl has so far not been determined by experiments since no catalytic intermediates were isolated. It can be expected that the basicity of the pyridyl subunit increases upon the introduction of the *para* substituent.[2] Under certain experimental conditions this could lead to the protonation of the dangling pyridine which would prevent it from participating in a base-assisted WNA mechanism.[1] However, this species would have a higher overall charge which would render the oxidation reactions required to reach the catalytically active $Ru^V{=}O$ state energetically more demanding. Taking these considerations into account and also to be consistent with our previous studies,[2,27] we simulate the O–O under neutral conditions i.e. neither any solvent molecule nor the pyridyl subunit were protonated at the beginning of our simulations.

So, how does the introduction of the methoxy group affect the O–O bond formation? The individual contributions of CV1 and CV2 to the MEP (see Figure 8) allow us to assess the influence of the pyridyl-modification on the O–O bond formation process. The projection of the MEP as a function of the $O_{oxo}-O_w$ distance (CV1) reveals three distinct phases of the entire process. In the initial phase, the nucleophile is oriented properly for the O–O bond

formation by forming a hydrogen bond with the intramolecular base, in the later referred to as pre-organization. In the second phase, the proton is partially transfered to the base while the $O_{oxo}-O_w$ distance remains constant at about 2.2 Å (proton-transfer). In the final phase, the length of the O–O bond is further reduced (O–O bond formation), while the proton is completely transfered to the base. Comparing the MEP energy profile of the two catalysts (see Table 2) reveals that the increased basicity primarily facilitates the first step of the bond formation process and has only a minor influence on the energetics of the proton-transfer and final O–O bond formation. The role of the intramolecular base therefore goes further than simply increasing the nucleophilicity of the attacking water molecules, since it is also responsible for properly orientating a solvent molecule in order to initialize an O–O bond formation. Comparing the MEPs as a function of CV2 leads to the same conclusion, namely that the largest energetic difference among the two catalysts is found in the initial phase of the reaction. However, the nature of the CV that monitors both the protonation state of the intramolecular base and the nucleophile make a clear distinction of different phases not expedient.

Table 2: Free energy differences obtained for the different phases of the MEP, if projected as function of CV1. All values given are in kJ/mol.

	phase	**{Ru(*p*OMePy5OMe)}**	**{Ru(Py5OMe)}**
1	pre-organization	15 ± 1	34 ± 1
2	proton-transfer	22 ± 1	25 ± 2
3	O–O bond formation	3 ± 1	9 ± 3
	TS	40 ± 2	69 ± 2

The effect of the increased basicity on the pre-organization step of the O–O bond formation can also be seen from the FES reweighted according to the minimal N–H distances (see Figure 9). On one hand, the FESs of both catalysts possess minima for the P, P1, P2 and P3 states in the same regions of the CV space, implying that altering the basicity of the intramolecular base does not significantly alter the reaction pathway. On the other hand, the local minima corresponding to the R state, i.e. free water, are found at signifi-

cantly shorter N–H distances: 2.0 Å in the case of **{Ru(*p*OMePy5OMe)}** vs. 3.0 Å for **{Ru(Py5OMe)}**. At the same time, the O_{oxo}–O_w distance is for both catalysts about 2.8 Å. This implies that the stronger base is able to attract the free nucleophile at larger N–H distances. Those weak hydrogen-bonding interactions facilitate the exploration of the configurational space in proximity of the reactive metal-oxo species, which inevitably leads to the O–O bond formation.

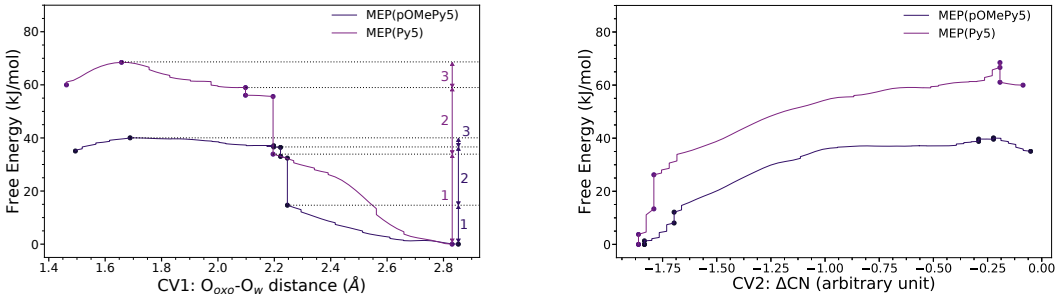

Figure 8: Free energy profile of the MEPs for the O–O bond formation as a function of CV1 (left) and CV2 (right) for the catalysts **{Ru(*p*OMePy5OMe)}** and **{Ru(Py5OMe)}**.[27] In the case of CV1, the reaction is subdivided into three distinctive phases, an analogous analysis in the case of CV2 is not expedient. The three phases of the reaction (pre-organization, proton-transfer and the O–O bond formation) are indicated by vertical arrows. The numbers correspond to the three phases: (1) pre-organization, (2) proton-transfer, and (3) O–O bond formation.

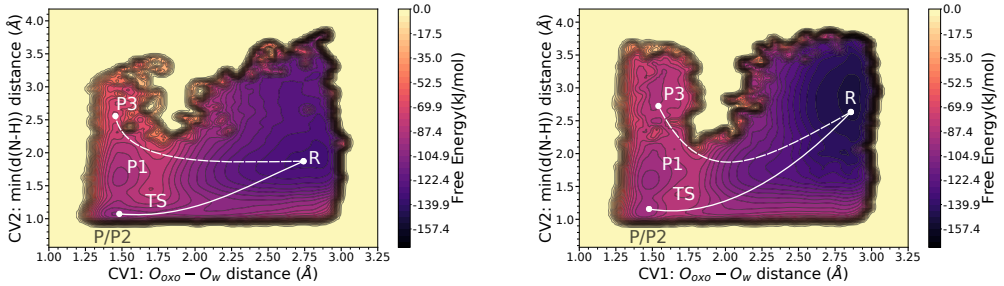

Figure 9: FESs of **{Ru(*p*OMePy5OMe)}** (left) and **{Ru(Py5OMe)}** (right), reweighted by the O_{oxo}–O_w distance (CV1) and the minimal N–H distance (CV2). The solid line serves as a visual guide line for the base-assisted WNA, while the dashed line is a guess for the base-independent WNA since there is no obvious MEP connecting the R and P3 state for both catalyst. The FES of **{Ru(Py5OMe)}** was obtained by post-processing data published by Schilling *et al.*[2]

The Bond Formation

In this section we will discuss the O−O bond formation by a base-assisted WNA. This reaction involves the formation of the $\sigma_{O_{oxo}-O_w}$ and the σ_{N-H} bond as well as the cleavage of the σ_{O_w-H} bond. LMOs were used to monitor the formation and breakage of the chemical bonds of interest during the course of the reaction (see Figure 10). Due to the open-shell nature of the simulations the alpha and beta channels are analyzed separately. Only the alpha channel is shown in Figure 10, an equivalent analysis for the beta channel as well as complete analysis using the PBE functional can be found in the Supplementary information (see Figures S4-S6).The main difference between the two channels is the presence of three LMOs describing the Ru−O_{oxo} bond in the case of the beta channel as opposed by only two LMOs in the alpha channel. The nature of LMOs involved in this bond can be categorized into σ, π and π-like (see Figure S7). The mixing of the σ and π orbitals is a known limitation of applied the Foster-Boys localization method.[64] However, this is of minor relevance as primarily the number of LMOs describing a chemical bond was analyzed and not the nature of the latter.

The evaluation of the LMOs was conducted for a sequence of frames with a total length of 1.7 ps that was extracted from the MetaD trajectory. In this sequence a reversible O−O bond formation event takes place. For every 50th frame (i.e. every 0.025 ps) the LMOs were analyzed as shown in Figure 10. At the beginning of the sequence, the nucleophile explores O−O distances slightly larger than 2 Å. For those states LMOs describing all bonds of interest can be found (i.e Ru−O_{oxo}, O_{oxo}−O_w, O_w−H, N−H). In the next phase, the O−O distance increases to 2.4 Å and the R state is reached, where the LMOs describing the O_{oxo}−O_w and the N−H bond are absent. The R state then continuously evolves into the P state, passing through transition regions where again all four LMOs are present. In the P state, the Ru−O_{oxo} bond is weakened as indicated by disappearance of a π-like LMO. The flexibility of the P state in terms of its protonation state can be seen from the temporary formation of an O_w−H bond. After remaining in P-like states for some time, the reaction

re-explores a series of TS-like states where the proton is primarily bound to the nucleophile. The presence or absence of LMOs describing the N−H bond highlights the importance of the intra-molecular base that interacts with the nucleophile not only in the P like states but also at larger $O_{oxo}-O_w$ distances. Monitoring the SENs[65] of the same bonds (see Figure S8) qualitatively leads to the same observations.

While this analysis gives a qualitative description of the reaction, it cannot give a definite answer to the question - how is the O−O bond formed i.e. is it a two or one electron process and which MOs are primarily involved. Han and Luber recently performed complete active space self-consistent field (CASSCF) simulations[71,72] for the O−O bond formation catalyzed by **{Ru(Py5OMe)}**. They found the O−O bond to be formed mainly by a two electron insertion as described by the determinant showing the largest weight in the CASSCF calculation.[73] The latter originates from the lone pair of the nucleophile and is inserted into the π^* orbital of the $Ru-O_{oxo}$. This is contrary to two consecutive one electron transfers as suggested for an iron-aqua complex by Bernasconi *et al.* using AIMD.[69]

The LMOs analysis used in this work implies for certain frames a single occupation of the $Ru-O_{oxo}$ bond. This, however is likely a consequence from our selection rule (i.e. contributions larger than 10%) rather an actual indication of a one-electron reaction. On the other hand, in analogy to Han and Luber, we observe the insertion of two electrons into the π^* MOs of the $Ru-O_{oxo}$ bond which results in the disappearance of a π-like LMO describing the $Ru-O_{oxo}$ bond in both spin channels.[73]

In addition to the LMOs and SENs we also analyzed Mulliken spin density differences although one should keep in mind possible associated shortcomings. Throughout the whole O−O bond formation the unpaired electron is shared between the metal center and the O_{oxo} ligand (see Figures S7). The unpaired electron is delocalized over the Ru−O bond for all intermediates. In agreement with the observations of Shao *et al.* both oxygen atoms of the hydroperoxo species in the P state possess some spin density indicating a localized electron over three centers of the R−OO fragment.[42]

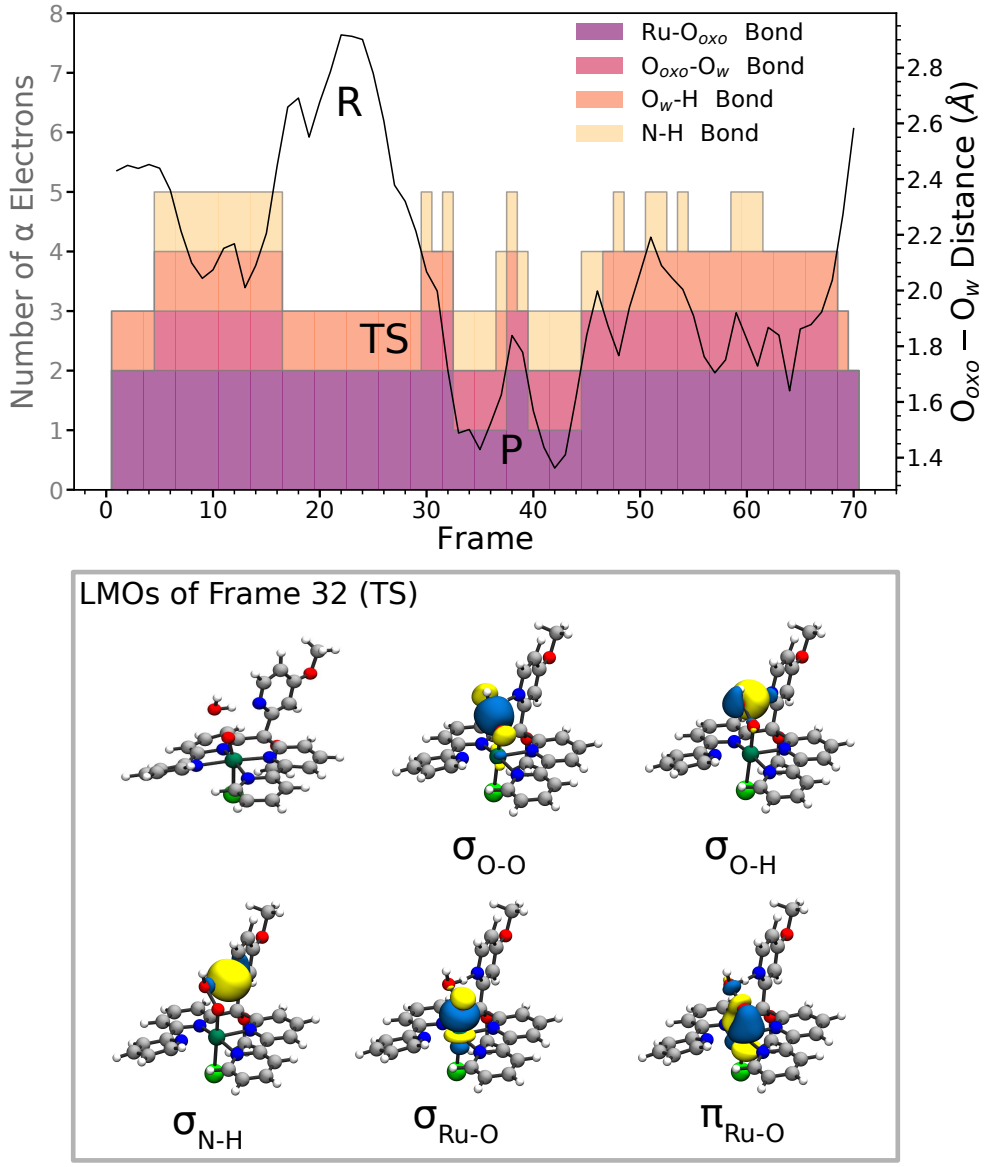

Figure 10: Visualization of the LMOs of the α channel that are characteristic for the base-assisted WNA. The atomistic structures along a representative reaction path are extracted from the MetaD simulation (see Figure 2 - 3rd trace from top, at about 56 ps)

Conclusions

The validity of rationally designed WOCs depends on the methods used to simulate their properties. Because of the high computational cost the inclusion of solvent dynamics and other effects at ambient temperature are often neglected. Accounting for such effects, we

obtained novel insights on the crucial interplay of a rationally designed WOC and its surrounding during the O – O bond formation.

Particularly, we have rationalized the effect of a modification to the Py5 ligand framework of a Ru-based WOC by applying forefront *ab initio* molecular dynamics in combination with enhanced sampling methods. In order to elucidate how the substitution at the pyridyl fragment enhances the basicity of the dangling base and alters the O – O bond formation, in particular its effect on the solvation shell, we performed MetaD simulations according to a simulation protocol established recently in our group.[27]

Applying the same combination of CVs to monitor the O – O bond formation and the protonation state of the nucleophile as well as the intramolecular base, we showed that the rationally designed WOC **{Ru(*p*OMePy5OMe)}** follows an analogous reaction path as **{Ru(Py5OMe)}**. This was achieved by identifying the MEP on the FES that was reconstructed from the MetaD simulation. The FES of **{Ru(*p*OMePy5OMe)}** features the same extrema as the ones of **{Ru(Py5OMe)}**. The main difference is the obvious energetic inequality of the base-assisted and base-independent reaction pathway, even without projecting the FES onto a three-dimensional reaction coordinate. This highlights the importance of the dangling base for the O – O bond formation reaction.

Comparing the energetics of the MEPs for the two catalysts we find, in agreement with our previous study applying static-DFT simulations, **{Ru(*p*OMePy5OMe)}** to have a lower activation energy than **{Ru(Py5OMe)}**. Despite the vast difference in terms of methods, a reasonable agreement between the activation energies obtained by the static-DFT simulations and the MetaD simulations is achieved.

Analyzing the energy profile of the MEPs for the two WOCs in terms of the contributions from the two CVs led to the identification of three phases of the reaction. At later stages of the MEPs, i.e. the proton-transfer and the O – O bond formation, the energetics of both catalysts was found to be similar. On the other hand, the energetics of the initial phase of the reaction was found to clearly favor **{Ru(*p*OMePy5OMe)}**. This phase is of high

relevance since it considers the formation of a hydrogen bond between the nucleophile and the base as well as the exploration of spatial orientation of the nucleophile with respect to the metal-oxo species that is suitable for the O−O bond formation.

In the case of **{Ru(*p*OMePy5OMe)}**, we identified the formation of a weak hydrogen bond interaction between the nucleophile and the intramolecular base to be the main cause for the lower activation energy. This intrinsic property could not have been observed by the static-DFT approach applied in our previous studies and therefore highlights the need to use techniques methods such as MetaD to properly describe reactions in the condensed phase.[2]

In addition to the comparison of the two WOCs, we also analyzed in detail the O−O bond formation for representative states of a selected bond formation event observed during the MetaD simulations. Monitoring the LMOs for each frame showed that the O−O bond formation process is a concerted mechanism that involves the formation of two bonds, while at the same time two other bonds are either broken or weakened. Analyzing the nature of the LMOs suggests a radical nature of the metal oxo species as well as a weakening of the $Ru-O_{oxo}$ bond as a consequence of the bond formation.

Overall, we have shown that *ab initio* molecular dynamics in combination with enhanced sampling methods and sophisticated consideration of the solvent environment can help rationalize the effects of ligand modifications, that go beyond modifying the electronic structure of catalysts involving specifically substrate-catalysts interactions.

The development of novel WOCs is currently still primarily driven by empiric observations. In order to come up with economically viable WOCs we cannot solely rely on such approaches. Informed design can potentially lead to the discovery of novel or the improvement of existing catalysts. While it is tempting to screen lots of potential candidates using computationally inexpensive approaches we still need to be aware of the limitations of those approaches. With this study we have shown that it is advisable to complement inexpensive approaches with more demanding simulations at ambient conditions including a more realistic description of the environment such as the solvent dynamics for a deeper understanding

of the reaction mechanism and the exploration of novel design criteria.

Supporting Information

Schematic representation of catalysts, definition of restraining potentials, block averages - dependencies on block number, LMO analysis of beta channel and employing the PBE functional, visualization of relevant LMOs, SEN analysis, description of structural features of key intermediates, Mulliken spin density differences analysis

Acknowledgment

The work has been supported by the University of Zurich, the university research priority program 'Solar Light to Chemical Energy Conversion' (LightChEC) and the Swiss National Science Foundation (grant no. PP00P2_170667). We thank the Swiss National Supercomputing Center for computing resources (project ID: s788 and s875).

References

(1) Gil-Sepulcre, M.; Böhler, M.; Schilling, M.; Bozoglian, F.; Bachmann, C.; Scherrer, D.; Fox, T.; Spingler, B.; Gimbert-Suriñach, C.; Alberto, R.; Bofill, R.; Sala, X.; Luber, S.; Richmond, C. J.; Llobet, A. Ruthenium Water Oxidation Catalysts based on Pentapyridyl Ligands. *ChemSusChem 10*, 4517–4525.

(2) Schilling, M.; Böhler, M.; Luber, S. Towards the rational design of the Py5-ligand framework for ruthenium-based water oxidation catalysts. *Dalton Trans.* **2018**, *47*, 10480–10490.

(3) Lai, W.; Cao, R.; Dong, G.; Shaik, S.; Yao, J.; Chen, H. Why Is Cobalt the Best

Transition Metal in Transition-Metal Hangman Corroles for O−O Bond Formation during Water Oxidation? *J. Phys. Chem. Lett.* **2012**, *3*, 2315–2319.

(4) Li, X.; Siegbahn, P. E. M. Water Oxidation Mechanism for Synthetic Co-Oxides with Small Nuclearity. *J. Am. Chem. Soc.* **2013**, *135*, 13804–13813.

(5) Tong, L.; Duan, L.; Xu, Y.; Privalov, T.; Sun, L. Structural Modifications of Mononuclear Ruthenium Complexes: A Combined Experimental and Theoretical Study on the Kinetics of Ruthenium-Catalyzed Water Oxidation. *Angw. Chem. Int. Ed.* **2011**, *50*, 445–449.

(6) Schilling, M.; Luber, S. Computational Modeling of Cobalt-Based Water Oxidation: Current Status and Future Challenges. *Front Chem* **2018**, *6*, 100.

(7) Schilling, M.; Patzke, G. R.; Hutter, J.; Luber, S. Computational investigation and design of cobalt aqua complexes for homogeneous water oxidation. *J. Phys. Chem. C* **2016**, *120*, 7966–7975.

(8) Zhang, B.; Sun, L. Ru-bda: Unique Molecular Water-Oxidation Catalysts with Distortion Induced Open Site and Negatively Charged Ligands. *J. Am. Chem. Soc.* **2019**, *141*, 5565–5580.

(9) Duan, L.; Araujo, C. M.; Ahlquist, M. S.; Sun, L. Highly efficient and robust molecular ruthenium catalysts for water oxidation. *Proc Natl Acad Sci USA* **2012**, 15584–15588.

(10) Kang, R.; Chen, K.; Yao, J.; Shaik, S.; Chen, H. Probing Ligand Effects on O−O Bond Formation of Ru-Catalyzed Water Oxidation: A Computational Survey. *Inorg. Chem.* **2014**, *53*, 7130–7136.

(11) Hessels, J.; Detz, R. J.; Koper, M. T. M.; Reek, J. N. H. Rational Design Rules for Molecular Water Oxidation Catalysts based on Scaling Relationships. *Chem. Eur. J.* **2017**, *23*, 16413–16418.

(12) Richmond, C. J.; Escayola, S.; Poater, A. Axial Ligand Effects of Ru-BDA Complexes in the O−O Bond Formation via the I2M Bimolecular Mechanism in Water Oxidation Catalysis. *Eur. J. Inorg. Chem.* **2019**, *2019*, 2101–2108.

(13) Zhang, G.; Chen, K.; Chen, H.; Yao, J.; Shaik, S. What Factors Control O2 Binding and Release Thermodynamics in Mononuclear Ruthenium Water Oxidation Catalysts? A Theoretical Exploration. *Inorg. Chem.* **2013**, *52*, 5088–5096.

(14) Jarvis, E. A.; Lee, B.; Neddenriep, B.; Shoemaker, W. Computational comparison of stepwise oxidation and O-O bond formation in mononuclear ruthenium water oxidation catalysts. *Chem. Phys.* **2013**, *417*, 8 – 16.

(15) Asaduzzaman, A. M.; Wasylenko, D.; Berlinguette, C. P.; Schreckenbach, G. Substitution Effects on the Water Oxidation of Ruthenium Catalysts: A Quantum-Chemical Look. *J. Phys. Chem. C* **2015**, *119*, 242–250.

(16) Okamura, M.; Masaoka, S. Design of Mononuclear Ruthenium Catalysts for Low-Overpotential Water Oxidation. *Chem. Asian J.* **2015**, *10*, 306–315.

(17) Durand, D. J.; Fey, N. Computational Ligand Descriptors for Catalyst Design. *Chem. Rev.* **2019**, *119*, 6561–6594.

(18) Foscato, M.; Jensen, V. R. Automated in Silico Design of Homogeneous Catalysts. *ACS Catal.* **2020**, *10*, 2354–2377.

(19) Schäfer, A.; Klamt, A.; Sattel, D.; Lohrenz, J. C. W.; Eckert, F. COSMO Implementation in TURBOMOLE: Extension of an efficient quantum chemical code towards liquid systems. *Phys. Chem. Chem. Phys.* **2000**, *2*, 2187–2193.

(20) Klamt, A. The COSMO and COSMO-RS solvation models. *WIREs Comput Mol Sci.* **2011**, *1*, 699–709.

(21) Hodel, F. H.; Deglmann, P.; Luber, S. Exploring Solvation Effects in Ligand-Exchange Reactions via Static and Dynamic Methods. *J. Chem. Theory Comput.* **2017**, *13*, 3348–3358.

(22) Evangelisti, F.; Moré, R.; Hodel, F.; Luber, S.; Patzke, G. R. 3d–4f $Co^{II}{}_3Ln(OR)_4$ Cubanes as Bio-Inspired Water Oxidation Catalysts. *J. Am. Chem. Soc.* **2015**, *137*, 11076–11084.

(23) Song, F.; Moré, R.; Schilling, M.; Smolentsev, G.; Azzaroli, N.; Fox, T.; Luber, S.; Patzke, G. R. $\{Co_4O_4\}$ and $\{Co_xNi4\text{-}xO_4\}$ Cubane Water Oxidation Catalysts as Surface Cut-Outs of Cobalt Oxides. *J. Am. Chem. Soc.* **2017**, *139*, 14198–14208.

(24) Schilling, M.; Hodel, F.; Luber, S. Discovery of open cubane-core Structures for biomimetic $\{LnCo_3(OR)_4\}$ Water Oxidation Catalysts. *ChemSusChem* **2017**, *10*, 4561–4569.

(25) Hodel, F. H.; Luber, S. What Influences the Water Oxidation Activity of a Bioinspired Molecular $Co^{II}{}_4O_4$ Cubane? An In-Depth Exploration of Catalytic Pathways. *ACS Catal.* **2016**, *6*, 1505–1517.

(26) Hodel, F. H.; Luber, S. Redox-Inert Cations Enhancing Water Oxidation Activity: The Crucial Role of Flexibility. *ACS Catal.* **2016**, *6*, 6750–6761.

(27) Schilling, M.; Cunha, R. A.; Luber, S. Zooming in on the O – O Bond Formation - an *ab initio* Molecular Dynamics Study Applying Enhanced Sampling Techniques. *J. Chem. Theory Comput.* **2020**, *14*.

(28) Sprik, M.; Ciccotti, G. Free energy from constrained molecular dynamics. *J. Chem. Phys.* **1998**, *109*, 7737–7744.

(29) Ciccotti, G.; Ferrario, M. Blue Moon Approach to Rare Events. *Mol. Sim.* **2004**, *30*, 787–793.

(30) Ciccotti, G.; Kapral, R.; Vanden-Eijnden, E. Blue Moon Sampling, Vectorial Reaction Coordinates, and Unbiased Constrained Dynamics. *ChemPlusChem* **2005**, *6*, 1809–1814.

(31) Laio, A.; Parrinello, M. Escaping free-energy minima. *Proc Natl Acad Sci USA* **2002**, *99*, 12562–12566.

(32) Laio, A.; Gervasio, F. L. Metadynamics: a method to simulate rare events and reconstruct the free energy in biophysics, chemistry and material science. *Rep. Prog. Phys.* **2008**, *71*, 126601.

(33) Barducci, A.; Bussi, G.; Parrinello, M. Well-Tempered Metadynamics: A Smoothly Converging and Tunable Free-Energy Method. *Phys. Rev. Lett.* **2008**, *100*, 020603.

(34) Barducci, A.; Bonomi, M.; Parrinello, M. Metadynamics. *Wiley Interdiscip. Rev.: Comput. Mol. Sci.* **2011**, *1*, 826–843.

(35) Sutto, L.; Marsili, S.; Gervasio, F. L. New advances in metadynamics. *Wiley Interdiscip. Rev.: Comput. Mol. Sci.* **2012**, *2*, 771–779.

(36) Nyhlén, J.; Duan, L.; Åkermark, B.; Sun, L.; Privalov, T. Evolution of O2 in a Seven-Coordinate RuIV Dimer Complex with a [HOHOH]- Bridge: A Computational Study. *Angw. Chem. Int. Ed.* **2010**, *49*, 1773–1777.

(37) Scherrer, D.; Schilling, M.; Luber, S.; Fox, T.; Spingler, B.; Alberto, R.; Richmond, C. J. Ruthenium water oxidation catalysts containing the non-planar tetradentate ligand, biisoquinoline dicarboxylic acid (biqaH2). *Dalton Trans.* **2016**, *45*, 19361–19367.

(38) Matheu, R.; Ertem, M. Z.; Benet-Buchholz, J.; Coronado, E.; Batista, V. S.; Sala, X.; Llobet, A. Intramolecular Proton Transfer Boosts Water Oxidation Catalyzed by a Ru Complex. *J. Am. Chem. Soc.* **2015**, *137*, 10786–10795.

(39) Vallés-Pardo, J. L.; Guijt, M. C.; Iannuzzi, M.; Joya, K. S.; de Groot, H. J. M.; Buda, F. Ab Initio Molecular Dynamics Study of Water Oxidation Reaction Pathways in Mono-Ru Catalysts. *Chem. Phys. Chem.* **2012**, *13*, 140–146.

(40) Piccinin, S.; Sartorel, A.; Aquilanti, G.; Goldoni, A.; Bonchio, M.; Fabris, S. Water oxidation surface mechanisms replicated by a totally inorganic tetraruthenium–oxo molecular complex. *Proc Natl Acad Sci USA* **2013**, *110*, 4917–4922.

(41) Govindarajan, N.; Tiwari, A.; Ensing, B.; Meijer, E. J. Impact of the Ligand Flexibility and Solvent on the O-O Bond Formation Step in a Highly Active Ruthenium Water Oxidation Catalyst. *Inorg. Chem.* **2018**, *57*, 13063–13066.

(42) Shao, Y.; de Ruiter, J. M.; de Groot, H. J. M.; Buda, F. Photocatalytic Water Splitting Cycle in a Dye-Catalyst Supramolecular Complex: Ab Initio Molecular Dynamics Simulations. *J. Phys. Chem. C* **2019**, *123*, 21403–21414.

(43) Shao, Y.; de Groot, H. J.; Buda, F. Proton Acceptor near the Active Site Lowers Dramatically the O–O Bond Formation Energy Barrier in Photocatalytic Water Splitting. *J. Phys. Chem. Lett.* **2019**, *10*, 7690–7697.

(44) Zhan, S.; Zou, R.; Ahlquist, M. S. G. Dynamics with Explicit Solvation Reveals Formation of the Prereactive Dimer as Sole Determining Factor for the Efficiency of Ru(bda)L2 Catalysts. *ACS Catal.* **2018**, *8*, 8642–8648.

(45) Zhan, S.; Ahlquist, M. S. G. Dynamics and Reactions of Molecular Ru Catalysts at Carbon Nanotube-Water Interfaces. *J. Am. Chem. Soc.* **2018**, *140*, 7498–7503.

(46) Govindarajan, N.; Meijer, E. J. Modeling the Catalyst Activation Step in a Metal–Ligand Radical Mechanism Based Water Oxidation System. *Inorganics* **2019**, *7*.

(47) Zhan, S.; De Gracia Triviño, J. A.; Ahlquist, M. S. G. The Carboxylate Ligand as an Oxide Relay in Catalytic Water Oxidation. *J. Am. Chem. Soc.* **2019**, *141*, 10247–10252.

(48) Pushkar, Y.; Pineda-Galvan, Y.; Ravari, A. K.; Otroshchenko, T.; Hartzler, D. A. Mechanism for O−O Bond Formation via Radical Coupling of Metal and Ligand Based Radicals: A New Pathway. *J. Am. Chem. Soc.* **2018**, *140*, 13538–13541.

(49) Moonshiram, D.; Pineda-Galvan, Y.; Erdman, D.; Palenik, M.; Zong, R.; Thummel, R.; Pushkar, Y. Uncovering the Role of Oxygen Atom Transfer in Ru-Based Catalytic Water Oxidation. *J. Am. Chem. Soc.* **2016**, *138*, 15605–15616.

(50) Pineda-Galvan, Y.; Ravari, A. K.; Shmakov, S.; Lifshits, L.; Kaveevivitchai, N.; Thummel, R.; Pushkar, Y. Detection of the site protected 7-coordinate Ru^{V}=O species and its chemical reactivity to enable catalytic water oxidation. *J. Catal.* **2019**, *375*, 1–7.

(51) Group, C. D. CP2K Program Package. `https://www.cp2k.org/`.

(52) VandeVondele, J.; Hutter, J. Gaussian basis sets for accurate calculations on molecular systems in gas and condensed phases. *J. Chem. Phys.* **2007**, *127*, 114105.

(53) Goedecker, S.; Teter, M.; Hutter, J. Separable dual-space Gaussian pseudopotentials. *Phys. Rev. B* **1996**, *54*, 1703–1710.

(54) Perdew, J. P.; Burke, K.; Ernzerhof, M. Generalized Gradient Approximation Made Simple. *Phys. Rev. Lett.* **1996**, *77*, 3865–3868.

(55) Grimme, S.; Antony, J.; Ehrlich, S.; Krieg, H. A consistent and accurate ab initio parametrization of density functional dispersion correction (DFT-D) for the 94 elements H-Pu. *J. Chem. Phys.* **2010**, *132*, 154104.

(56) Nosé, S. A unified formulation of the constant temperature molecular dynamics methods. *J. Chem. Phys.* **1984**, *81*, 511–519.

(57) Nosé, S. A molecular dynamics method for simulations in the canonical ensemble. *Mol. Phys.* **1984**, *52*, 255–268.

(58) W. Humphrey, K. S., A. Dalke VMD: visual molecular dynamics. *J Mol Graph* **1996**, *14*, 33–38.

(59) Giorgino, T.; Laio, A.; Rodriguez, A. METAGUI 3: A graphical user interface for choosing the collective variables in molecular dynamics simulations. *Comput. Phys. Commun.* **2017**, *217*, 204–209.

(60) Ahlrichs, R.; Bär, M.; Häser, M.; Horn, H.; Kölmel, C. Electronic structure calculations on workstation computers: The program system turbomole. *Chem. Phys. Lett.* **1989**, *162*, 165 – 169.

(61) Becke, A. D. Density-functional exchange-energy approximation with correct asymptotic behavior. *Phys. Rev. A* **1988**, *38*, 3098–3100.

(62) Perdew, J. P. Density-functional approximation for the correlation energy of the inhomogeneous electron gas. *Phys. Rev. B* **1986**, *33*, 8822–8824.

(63) Weigend, F.; Ahlrichs, R. Balanced basis sets of split valence, triple zeta valence and quadruple zeta valence quality for H to Rn: Design and assessment of accuracy. *Phys. Chem. Chem. Phys.* **2005**, *7*, 3297–3305.

(64) Foster, J. M.; Boys, S. F. Canonical Configurational Interaction Procedure. *Rev. Mod. Phys* **1960**, *32*, 300–302.

(65) Ehrhardt, C.; Ahlrichs, R. Population analysis based on occupation numbers II. Relationship between shared electron numbers and bond energies and characterization of hypervalent contributions. *Theor. Chim. Acta* **1985**, *68*, 231–245.

(66) Tribello, G. A.; Bonomi, M.; Branduardi, D.; Camilloni, C.; Bussi, G. PLUMED 2: New feathers for an old bird. *Comput. Phys. Commun.* **2014**, *185*, 604 – 613.

(67) Raiteri, P.; Laio, A.; Gervasio, F. L.; Micheletti, C.; Parrinello, M. Efficient Reconstruction of Complex Free Energy Landscapes by Multiple Walkers Metadynamics. *J. Phys. Chem. B* **2006**, *110*, 3533–3539.

(68) Marcos-Alcalde, I. n.; Setoain, J.; Mendieta-Moreno, J. I.; Mendieta, J.; Gómez-Puertas, P. MEPSA: minimum energy pathway analysis for energy landscapes. *Bioinformatics* **2015**, *31*, 3853–3855.

(69) Bernasconi, L.; Kazaryan, A.; Belanzoni, P.; Baerends, E. J. Catalytic Oxidation of Water with High-Spin Iron(IV)–Oxo Species: Role of the Water Solvent. *ACS Catalysis* **2017**, *7*, 4018–4025.

(70) Öğretir, C.; Özöğüt, D.; Yarligan, S.; Arslan, T. Quantum chemical studies on acidity-basicity behaviours of some substituted pyridine derivatives. *J. Mol. Struct. THEOCHEM* **2006**, *759*, 73–78.

(71) Roos, B. O.; Taylor, P. R.; Sigbahn, P. E. M. A complete active space SCF method (CASSCF) using a density matrix formulated super-CI approach. *Chem. Phys.* **1980**, *48*, 157–173.

(72) Siegbahn, P. E. M.; Almlöf, J.; Heiberg, A.; Roos, B. O. The complete active space SCF (CASSCF) method in a Newton–Raphson formulation with application to the HNO molecule. *J. Chem. Phys.* **1981**, *74*, 2384–2396.

(73) Han, R.; Luber, S. Investigating the oxygen-oxygen bond formation using complete active space analysis of a reaction pathway. *J. Comput. Chem.* **2020**, 10.1002/jcc.26201.